

pubs.acs.org/JPCC Article

Coupling between Harmonic Vibrations Influences Quantum Beating Signatures in Two-Dimensional Electronic Spectra

Published as part of The Journal of Physical Chemistry virtual special issue "Quantum Coherent Phenomena in Energy Harvesting and Storage".

Jonathan D. Schultz, Taeyeon Kim, James P. O'Connor, Ryan M. Young, and Michael R. Wasielewski*



Cite This: J. Phys. Chem. C 2022, 126, 120-131



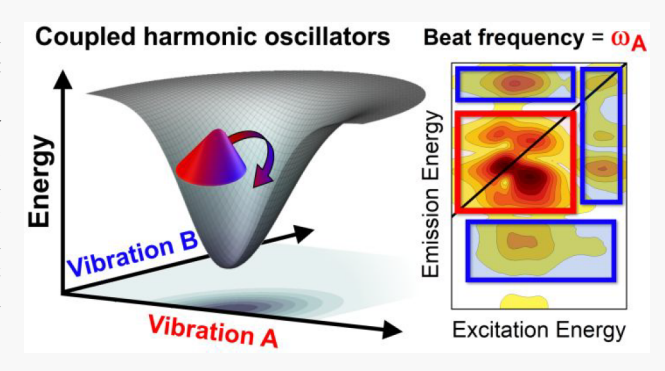
ACCESS

III Metrics & More

Article Recommendations

Supporting Information

ABSTRACT: Launching and tracking wavepacket dynamics with two-dimensional electronic spectroscopy (2DES) provides insight into the complex interactions that underlie coherent processes within photoactive materials. With the ever-growing interest in how electronic-vibrational (vibronic) interactions direct ultrafast photophysics, methods for translating 2DES results into meaningful descriptions of the molecular potential energy landscape must evolve correspondingly. The interpretation of quantum beatmaps, which provide direct insight into the intra- and interchromophoric couplings within a chemical system, frequently relies on physical models that account for a single nuclear coordinate. However, several recent works suggest that coupling between wavepackets



borne from several different vibrational motions affects 2DES data in meaningful ways. We build upon these insights by directly comparing simulations using single- and multicomponent vibronic Hamiltonians against experimental 2DES results from the organic semiconductors terrylenediimide and ITIC, as well as the biomedical dyes methylene blue and Nile blue A. We show that the experimental beatmaps and Fourier power spectra are well-reproduced when both low- and high-frequency vibrational motions are included in the simulation. Moreover, we demonstrate that the interaction of harmonic wavepackets increases quantum beat amplitudes in the positive-frequency rephasing signals, which significantly complicates standard methods for separating ground- and excited-state vibrational coherence signatures from 2DES data. These findings illustrate that coupling between purely harmonic vibrational wavepackets can have significant and prevalent effects on experimental 2DES results.

■ INTRODUCTION

The interplay of nuclear and electronic coordinates in driving photochemical reactions offers a platform for external control of chemical dynamics on the molecular scale. 1-3 Coupled electronic-vibrational (vibronic) degrees of freedom have been shown to underlie several important photochemical reactions such as energy⁴⁻¹⁰ and charge transfer, 11-22 singlet fission, ^{23–29} excimer formation, ^{30,31} phase transitions, ^{32,33} and solvation dynamics.³⁴ While many techniques allow insight into the vibronic configurations of multichromophoric systems, disentangling the key contributors to reaction coordinates remains challenging. ^{17,35} The extensive frequencyand time-domain information afforded by two-dimensional electronic spectroscopy (2DES) has been particularly insightful for uncovering vibronic couplings and their connections to electronic dynamics. 1,6,7,16,22,23,25,36-39 In addition, the growing accessibility^{8,40} and range of experimental 2DES implementations⁴¹ make it a powerful tool for bridging disciplinary gaps that have historically hampered progress

toward engineering vibronic coherence within rationally designed molecular systems.^{3,42}

Owing to the temporally short and spectrally broad pulses that are required for 2DES, this nonlinear spectroscopic technique is able to launch and track the evolution of both populations and coherences among the quantum mechanical states of a molecular ensemble. While 2DES spectra are often analyzed with respect to excitation (ω_1) and emission (ω_3) dimensions at specified waiting time delays (t_2) , as portrayed in the top panel of Figure 1, information explicitly about coherence phenomena can be extracted by fitting and subtracting population dynamics in the t_2 domain (middle panel of Figure 1) and subsequently performing a Fourier

Received: November 1, 2021 Revised: December 16, 2021 Published: January 4, 2022





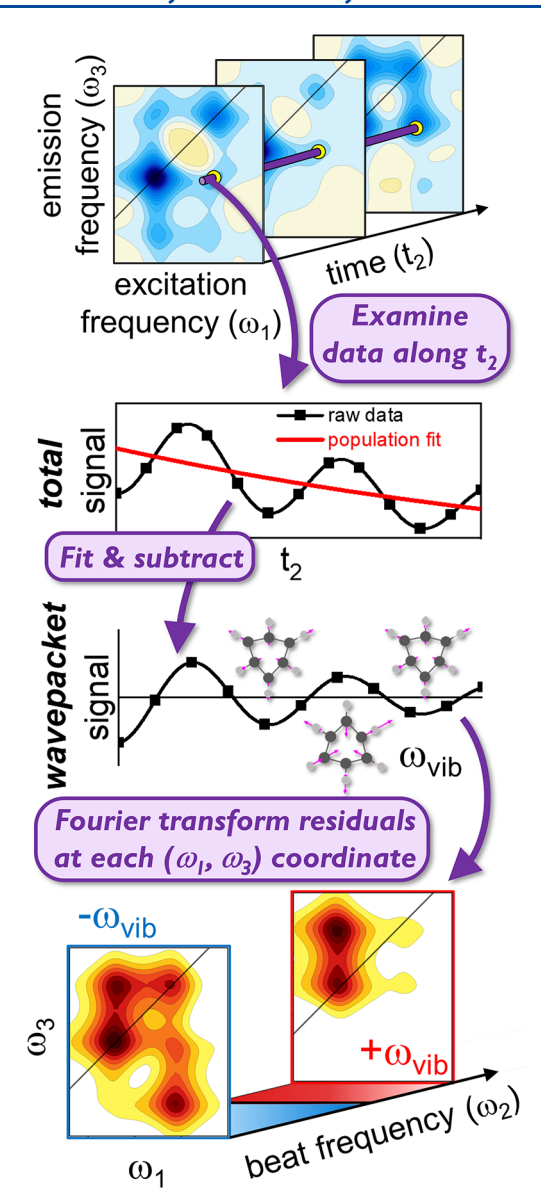


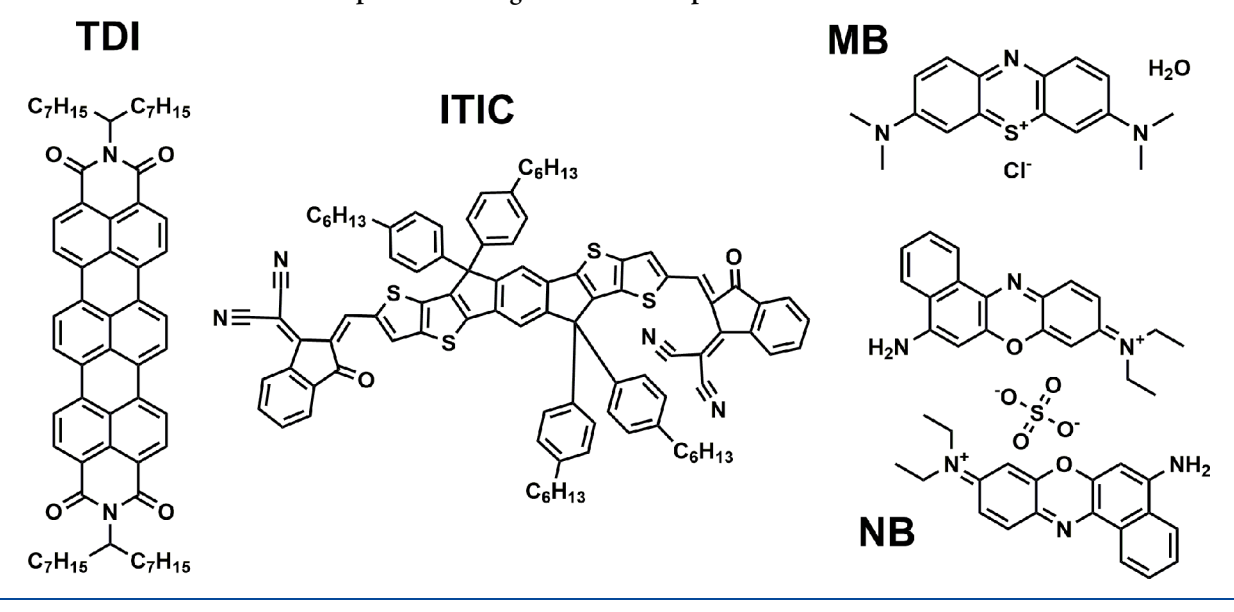
Figure 1. 2DES produces signals as a function of excitation (pump) and emission (probe) frequencies and the waiting time (t_2) . The signal intensity along t_2 reveals population (nonoscillatory) and coherence (oscillatory) dynamics. Fitting and subtracting the former yields isolated wavepacket signals. Quantum beatmaps are obtained by repeating this process at all (ω_1, ω_3) coordinates and Fourier transforming the residuals. The features in each ω_2 beatmap are directly linked to the underlying nature of the system.

transformation of the residuals over t_2 . ⁴⁴ In the product pure frequency-domain $(\omega_1, \omega_2, \omega_3)$ representation, as shown in the lower panel of Figure 1, slices in the dataspace taken at constant ω_2 values indicate the amplitude of specific coherent signal oscillations, or quantum beats, as a function of excitation and emission energies. These so-called quantum beatmaps offer rich topological insight into the potential energy landscape of a molecular system and have been used to probe vibronically coherent energy transfer in photosynthetic complexes, ^{45,46} reveal nuclear motions that enable important photochemical transformations in organic photovoltaic systems, ^{4,11,16,23,25,26,47} and explore the possibility of harnessing vibronic coupling as a design parameter in chemical technologies. ^{1,32,33,48–51}

While 2DES beatmaps help to parse the fundamental parameter space of complex chemical ensembles, translating these maps into meaningful conclusions is by no means trivial. The single displaced harmonic oscillator (DHO) model is often assumed for simplicity when rationalizing patterns within beatmaps while accounting for both electronic and nuclear degrees of freedom. 52-54 The validity of this assumption, however, is brought into question by an increasing number of works that highlight the need to account for multiple vibrational coordinates in the mechanisms of a variety of ultrafast photochemical phenomena. 7,14,26,28,55-59 While measuring couplings between nuclear motions is a central focus of many experimental techniques, such as multidimensional infrared, 60,61 electronic-vibrational, 62-67 vibrational-electronic, 62,63,68 and impulsive stimulated Raman spectroscopies, 69 the effects of such coupling are largely ignored in the analysis of 2DES beatmaps. Recent theoretical⁷⁰ and experimental studies^{55,58} have attributed marked deviations from the single-DHO model of 2DES beatmaps to wavepacket motion along coupled nuclear coordinates. Nevertheless, the shortage of direct comparisons between theoretical and experimental results limits the accuracy and general applicability of models that account for vibrational coupling in calculating 2DES beatmaps. As the connections between 2DES and the rational design of quantum technologies continue to expand, 3,50 the effects and prevalence of coupled vibrational coordinates must be clarified.

Here, we use a joint experimental-theoretical approach to test the ability of the single-DHO versus multiple-DHO formalisms to reproduce experimental 2DES results from an array of chromophores, namely terrylenediimide (TDI), ITIC, methylene blue (MB), and Nile blue A (NB). Both TDI and ITIC have applications in organic photovoltaics as singlet fission sensitizers⁷¹⁻⁷³ and nonfullerene electron acceptors, 74,75 respectively, while MB and NB are important dyes to the biomedical community. 76,77 We first focus on comparisons between simulated quantum beatmaps for TDI, using both single- and multiple-DHO Hamiltonians, and experimental 2DES results. We show unambiguously that accounting for multiple unique vibrations significantly increases the accuracy of the simulation in capturing patterns within the experimental beatmaps. We attribute this agreement, which is achieved without treatment of anharmonicity, to coupling between multiple linearly displaced harmonic oscillators. Additional experiments indicate that deviations from the single-DHO formalism are also prevalent in the beatmaps for ITIC, MB, and NB, which illustrates the broad influence of harmonically coupled vibrations on 2DES results. Furthermore, we demonstrate that the multiple-DHO model increases the amplitude of ground-state vibrational signatures in the positive-frequency rephasing beatmaps in comparison to those predicted by the single-DHO formalism. Thus, harmonic coupling between vibrations may significantly complicate established procedures for separating signals from groundand excited-state vibrational coherence, which highlights the importance of considering multiple nuclear coordinates when drawing conclusions from 2DES beatmaps, especially when multiple Franck-Condon (FC)-active modes are present. Taken together, these results demonstrate that 2DES simulations treating multiple vibrations on the same footing can increase the extent to which features in experimental quantum beatmaps can be linked to the fine vibronic structure

Scheme 1. Structures for the Chromophores Investigated in This Report



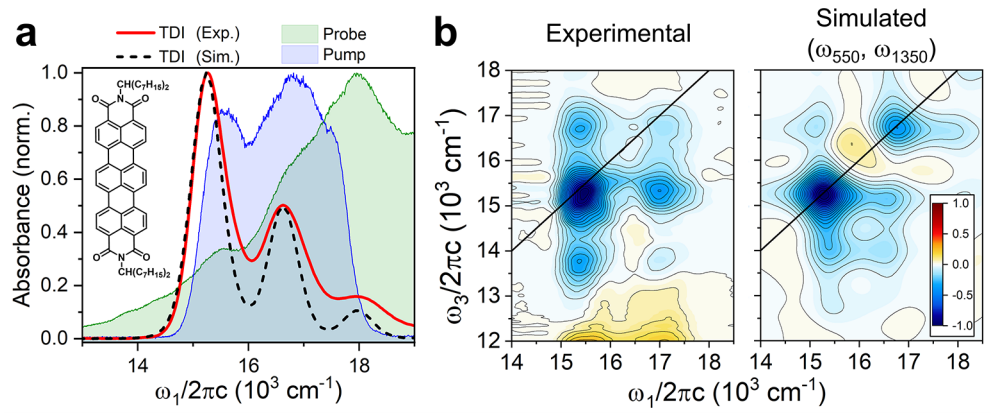


Figure 2. (a) Normalized experimental (Exp.) and simulated (Sim.) steady-state absorption spectra for TDI (structure inset) with 2DES pump and probe spectra superimposed. (b) Experimental and simulated 2DES spectra near $t_2 = 100$ fs. Contours are plotted at 5% intervals with 10% contour lines darkened. Experimental spectra were collected with the sample dissolved in THF at room temperature.

of the molecular Hamiltonian, even for complex, solution-phase ensembles.

METHODS

Materials. Terrylene-3,4:11,12-bis(dicarboximide) (TDI) was prepared according to literature procedures. ⁷³ 3,7-Bis(dimethylamino)phenazathionium chloride (MB) and the nonfullerene acceptor 2,2'-[[6,6,12,12-tetrakis(4-hexylphenyl)-6,12-dihydrodithieno[2,3-d:2',3'-d']-s-indaceno[1,2-b:5,6-b']-dithiophene-2,8-diyl]bis[methylidyne(3-oxo-1*H*-indene-2,1(3H)-diylidene)]]bis[propanedinitrile] (ITIC) were purchased from Sigma-Aldrich and used without any further purification. 5-Amino-9-(diethylamino)-benzo[a]phenoxazin-7-ium perchlorate (NB) was purchased from Eastman and used without further purification. Scheme 1 illustrates molecular structures for all compounds included in this study.

Optical Spectroscopy. Steady-state UV-vis absorption spectra for room temperature solutions of each dye molecule were collected using a Shimadzu UV-1800 spectrophotometer. Solutions were prepared with optical densities ranging from 0.2 to 0.8 OD in glass cuvettes with a 1 mm path length for the following solute/solvent pairs: TDI/tetrahydrofuran (THF),

MB/water (deionized), NB/ethanol, and ITIC/dichloromethane (DCM). Both THF and DCM were dried using a Glass Contour solvent system.

2DES experiments were conducted using an apparatus detailed in our previous works 78,79 and employed pump pulses centered near 16650 cm⁻¹ (Figure 2), which spanned 3390 cm⁻¹ baseline-to-baseline (defined as 5% of the maximum intensity). Using an acousto-optic modulator-based pulse shaper, 80 we compressed these pulses to between 10 and 15 fs in duration (Figure S1) and focused them on the sample position with a dispersion-corrected white light (WL) probe spanning approximately 500-1000 nm. We collected a series of 2DES spectra in the pump-probe geometry as a function of the delay between the second pump and the probe pulses (the waiting time, t_2) to analyze wavepacket dynamics. This delay was scanned from approximately -100 to 1600 fs across several trials with either 5 or 8 fs step sizes. To extract the absorptive, rephasing, and nonrephasing contributions to the pump-probe geometry 2DES signals, we employed well-documented phase cycling procedures. 81,82 Quantum beatmaps were extracted from the data per our previously published protocols^{23,79,83} in conjunction with an existing package⁸⁴ used to increase the efficiency of subtracting

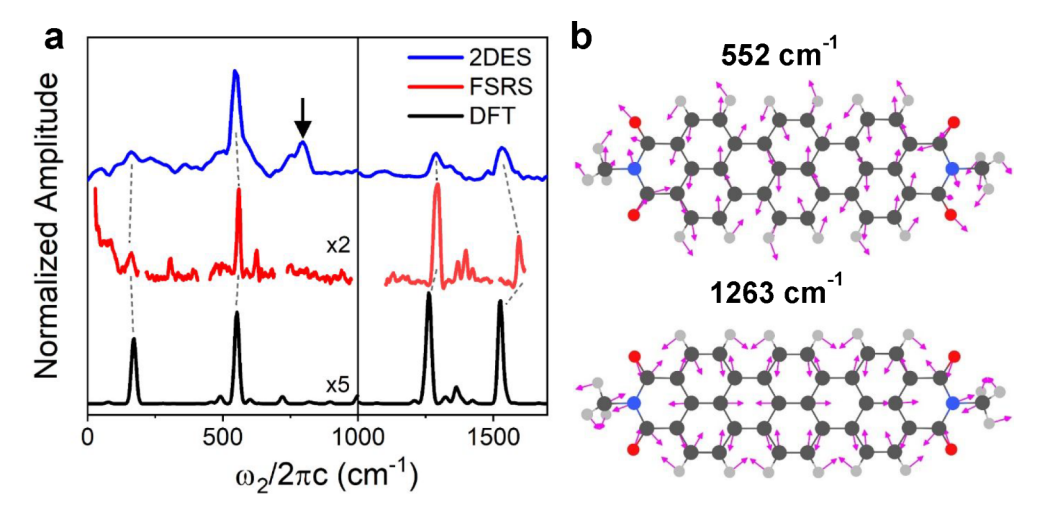


Figure 3. Comparison of (a) power spectra obtained via 2DES, FSRS, and resonance-Raman DFT calculations and (b) the calculated nuclear motions that are represented within the multiple-DHO model for TDI. The solid vertical line in panel a indicates the region (left) over which the indications of magnification are applicable. The dotted lines in panel a connect features that are commonly observed through all three methods, accounting for minor frequency shifts.

population dynamics. Samples for transient experiments were prepared as described above. Refer to the Supporting Information (SI) for further details regarding the apparatus, pulse characterization, experimental parameters and replicate results (Figures S4, S6, S12, and S13), postprocessing, and additional experiments (Figures S7, S8, S10).

We performed femtosecond stimulated Raman scattering (FSRS) experiments with a previously described laser system. The narrowband (approximately $15~\rm cm^{-1}$) Raman pump was tuned to be preresonant with the 0-0 vibronic transition visible in the steady-state linear absorption for TDI (Figure 2a). Samples for these experiments were prepared as described above, but in cuvettes with a 2 mm path length.

Theoretical Modeling. We employed an original MATLAB toolbox^{23,79} to generate a Holstein-form Hamiltonian (eq S1) with an arbitrary number of vibrations and propagate the system through real time in response to electromagnetic perturbations. We treated system-bath interactions with a stochastic fluctuation model⁸⁶ and fixed the phenomenological parameters for all simulations (eq S11), which means that the microscopic mechanism(s) for variations between our simulations are solely based on the structure of the system Hamiltonian. In this work, we examine the effects of including either one or two DHOs within the system Hamiltonian on the resulting 2DES quantum beatmaps. Importantly, all DHOs are treated on equal footing. On the basis of our previous study of TDI,²³ we explored the 550 and 1350 cm⁻¹ vibrations that are evident in the 2DES power spectra and linear response of TDI, respectively. We parametrized these vibronic Hamiltonians based on the degree to which the simulations reproduce the steady-state absorption (Figure S2) and 2DES spectra at constant waiting times for TDI, as summarized in Table S1. By enforcing time-ordering, we simulated each component of the four-wave-mixing signal separately. These components are the rephasing and nonrephasing contributions to the ground-state bleach (GSB), stimulated emission (SE), and excited-state absorption (ESA) signal generation pathways (eqs S5-S10). Refer to the SI for additional details regarding the theoretical model and data processing methods.

Density Functional Theory Computations. DFT calculations were performed using the Amsterdam Density Functional (ADF) software package. We employed the BP86 functional in conjunction with a DZP basis set to compute optimized geometries, normal modes, and resonance Raman spectra of TDI in silico. Frequencies were scaled to account for anharmonicity using parameters reported in a previous study.⁸⁷

■ RESULTS AND DISCUSSION

Experimental and Theoretical TDI Response Comparisons. We first investigated the linear response of TDI. Figure 2a shows the experimental TDI steady-state absorption spectrum, in addition to the spectra of the pulses used to perform 2DES measurements. The TDI absorption spectrum features a progression of vibronic peaks with an average spacing of 1360 cm⁻¹ (15260, 16600, and 17980 cm⁻¹). While we have previously shown that numerous vibrations are coupled to the $S_1 \leftarrow S_0$ electronic transition of TDI,²³ we dressed the multiple-DHO Hamiltonian with 550 and 1350 cm⁻¹ vibrations to simulate the linear response (Figure S2). This allowed us to maintain reasonable computational time while still representing both low- and high-frequency regimes within the simulations. We found that the Huang-Rhys (HR) factor (λ^2) for the 1350 cm⁻¹ vibration ($\lambda^2 = 0.42$) is more than three times larger than that of the 550 cm^{-1} vibration (λ^2 = 0.13), which is a common outcome when comparing the HR factors for high- and low-frequency vibrations of organic chromophores.⁸⁸ Refer to Table S1 in the SI for a full compilation of parameters used in these simulations.

Using the parameters obtained through reproducing the experimental linear response with the multiple-DHO simulation, we extended our model to calculate the third-order response. The left panel of Figure 2b illustrates an experimental 2DES spectrum collected at $t_2 = 100$ fs (S_1 lifetime = 2.5 ns in CH₂Cl₂),⁷³ which agrees with our previous 2DES studies of TDI-based compounds.^{23,78} Briefly, a grid of intense, negative-signed peaks surrounds the diagonal $\omega_3 = \omega_1$ line. The peaks near the diagonal (ω_1 , ω_3) = (15440, 15240 cm⁻¹) and (17070, 16730 cm⁻¹) arise from both ground state (S_0) bleach (GSB) and excited-state (S_1) stimulated emission (SE) from the 0–0 and 0–1 vibronic transitions of the 1350

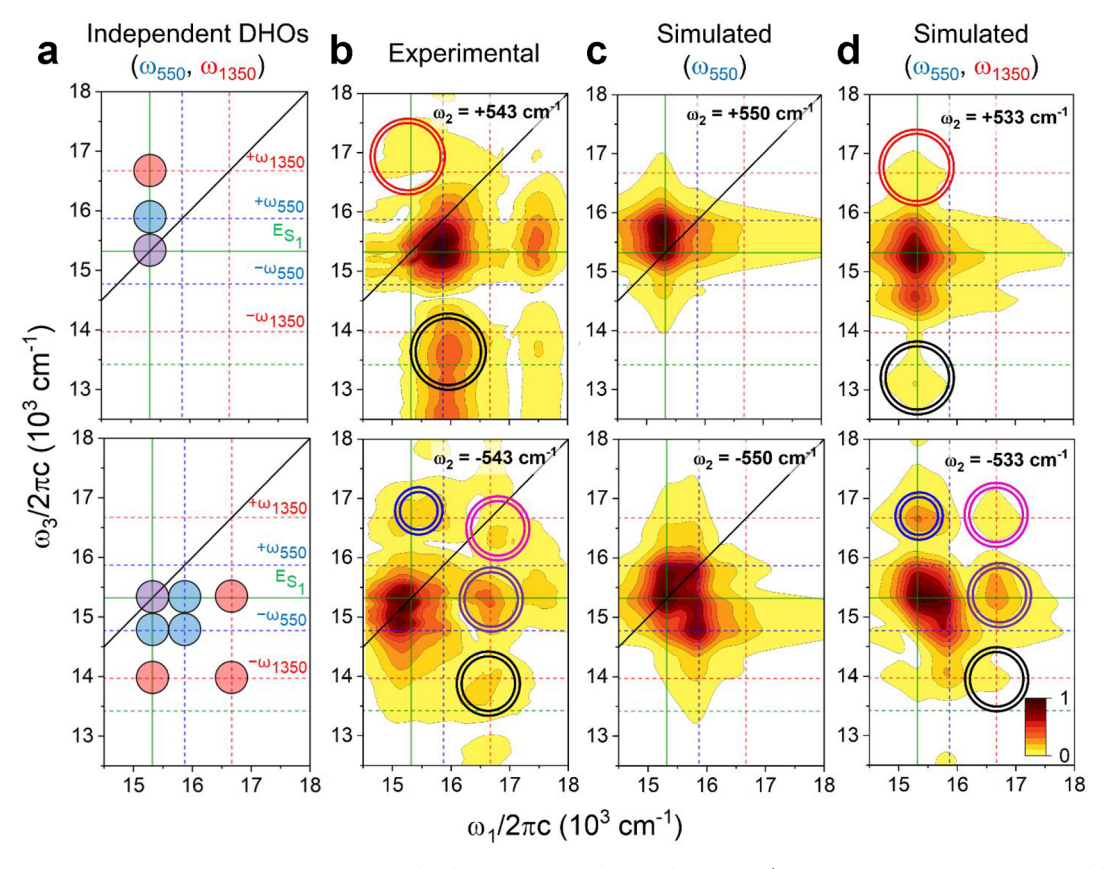


Figure 4. Rephasing quantum beatmaps for the positive (top) and negative (bottom) 550 cm⁻¹ beat frequencies obtained from (a) a schematic picture of individual 550 and 1350 cm⁻¹ vibrations, (b) experimental 2DES data, and third-order signals simulated with the (c) single-DHO simulations, and (d) multiple-DHO Hamiltonians. The solid green lines indicate the 0–0 singlet electronic transition energy for all vibrations. Dotted lines indicate energy that represents either one or two frequency quanta away from the 0–0 singlet transition energy in either the pump (vertical lines) or probe (horizontal lines) axis for the 550 (blue), 1350 (red), and combination (green) bands. Solid circles in panel a indicate regions with nonzero beating amplitude (color coded according to origin vibration: ω_{550} = blue, ω_{1350} = red, overlap of ω_{550} and ω_{1350} = purple) while hollow circles in panels b and d highlight features that are not accounted for within the single-DHO approximation.

cm⁻¹ mode, respectively. We attribute the 300 cm⁻¹ increase in the spacing between these peaks in the pump dimension relative to the 1350 cm⁻¹ vibration to the spectral bandwidth of the pump pulse. As anticipated, these transitions also exhibit crosspeaks near (15390, 16750 cm⁻¹) and (17000, 15330 cm⁻¹). SE crosspeaks from the 1350 cm⁻¹ mode are also observed near (15370, 13740 cm⁻¹) and (17030, 13820 cm⁻¹). In addition, the tails of two positive ESA peaks are visible at the bottom edge of the ω_3 axis and are attributed to an $S_n \leftarrow S_1$ transition. While we include this transition in our simulations (Figures S4 and S17), we draw our primary conclusions from the pump-probe frequency regime portrayed by the spectra in Figure 2b. (See the SI for further details.) As shown by the right panel of Figure 2b, our simulation yields excellent agreement with the experimental 2D spectrum, with exception of the finite bandwidth in the latter. While the experimental spectrum represents a convolution of the third-order response and the pump spectrum, we maintain generality in our simulations by centering discussions around the unconvoluted response. We note however that this convolution is more important to consider when the pump-bandwidth spans only a fraction of the steady-state absorption spectrum of the solute.⁸⁹

Signatures of Wavepacket Motion from TDI. As shown by the blue trace in Figure 3a, we observe clear wavepacket motion from TDI manifested as numerous quantum beats in the 2DES data near frequencies $\omega_2 = 160$, 550, 800, 1300, and

1550 cm⁻¹. Since GSB and SE signals overlap substantially near the diagonal line in a 2DES data set, these beats likely originate from a combination of both ground- (S_0) and excited-state (S₁) vibrational coherences.⁵³ The ground-state contribution is supported by the excellent agreement between most features and the spectra obtained from FSRS and resonance-Raman DFT. Two key differences are noteworthy, however. First, the ω_2 = 800 cm⁻¹ peak in the 2DES power spectrum (observed between 800 and 860 cm⁻¹ in additional independent measurements (Figures S7 and S8)) is completely absent in both the FSRS and DFT spectra. This discrepancy indicates that this mode stems predominantly from the excitedstate wavepacket evolution. This feature could be rationalized by a significant Duschinsky rotation 90 or as a combination band due to anharmonic coupling. However, we note that both of these phenomena have been observed to manifest in experimental FSRS spectra. 91 The second difference between the spectra in Figure 3a is the relative amplitude of the lowand high-frequency motions, which is seen most clearly by comparing the ratio of the 550 and 1300 cm⁻¹ modes in each spectrum. While FSRS and the DFT computations indicate that the 1300 cm⁻¹ vibration couples more strongly to the S₁ \leftarrow S₀ transition than the 550 cm⁻¹ mode, the 2DES power spectrum suggests the opposite. Since we know this is incorrect considering the 1300 cm⁻¹ vibration is likely responsible for the prominent 1350 cm⁻¹ vibronic progression in the linear

absorption spectrum (Figure 2a), we attribute this discrepancy to effects of the finite pulse duration in launching and probing wavepacket motion. ⁹²

Although we observe that more than four TDI vibrations have significant FC activity, we restrict our multiple-DHO simulations to the inclusion of 1350 and 550 cm⁻¹ vibrations for several reasons. First, the former mode is dominant in the FSRS, DFT, and linear absorption spectra, whereas the latter modulates the 2DES signals with the strongest intensity. Second, previous works report that the effects of interference between wavepacket motions are most evident when a significant difference exists between their carrier frequencies. S5,70 Thus, our choice of both low- (<1000 cm⁻¹) and high-frequency (>1000 cm⁻¹) vibrations allows us to examine the generality of this finding.

Comparisons of Experimental and Theoretical TDI Quantum Beatmaps. A significant advantage of using 2DES to study wavepacket dynamics is the ability to analyze both the rephasing and nonrephasing contributions to the third-order signal, which serves to isolate overlapping oscillatory signals that may otherwise interfere with each other. Signals also allows additional information to be obtained by examining both the positive- and negative-signed beat frequencies. We therefore focus our analysis on the rephasing portions of the experimental and theoretical signals, while the nonrephasing (Figure S12) and absorptive (Figure S10) counterparts are provided in the SI.

Significant effort has been placed on linking quantum beatmaps to particular molecular models, both for the $1D^{4,14,52,94,98,99}$ and 2D implementations of ultrafast electronic spectroscopy. 6,25,37,45,49,53,70,77,95,96,100 In the simplest case of an isolated chromophore, the single-DHO model predicts features in the positive and negative frequency rephasing 2DES beatmaps spaced by the frequency of the harmonic oscillator, 53 as shown in Figure 4a for both the 550 and 1350 $\,\mathrm{cm}^{-1}$ vibrations (assuming their wavepacket motions are completely independent). In contrast to our simulations, which include five vibrational quanta for each electronic state, these depictions consider only a single quantum of the nuclear motion on both the ground- and excited-electronic states. The experimental rephasing beatmaps for the $\omega_2 = +543$ (top) and -543 cm⁻¹ (bottom) are shown in Figure 4b, where deviations from the schematics in Figure 4a are immediately evident. Namely, we observe several peaks in the beatmap located greater than one energy quantum away from the diagonal line. While it is tempting to assign these features to signal pathways involving higher vibrational states of the 550 cm $^{-1}$ vibration (ν > 1), our simulations using the single-DHO Hamiltonian do not predict such behavior (Figure 4c). Since the $0-\nu_n$ FC factor decreases rapidly as $\nu_{\rm n}$ increases, quantum beats originating from a single vibrational motion dramatically decrease in amplitude as the distance from the 0-0 vertical transition energy in the pump-probe frequency space increases.

In stark contrast to the theoretical single-DHO results, the rephasing beatmaps obtained from the multiple-DHO simulation (Figure 4d) exhibit remarkable agreement with the experimental beatmaps, as highlighted by the colored circles in Figure 4 both panels b and d. Comparing panels b and d to the schematic in Figure 4a suggests that the 550 cm⁻¹ beatmap draws amplitude from both the 550 and 1350 cm⁻¹ modes. On the basis of recent theoretical predictions, ⁷⁰ this observation suggests that interference between the 550 and 1350 cm⁻¹ modes is responsible for the marked deviations

from the expectations from the traditional single-DHO model. Comparisons between our experimental and simulated absorptive beatmaps (Figure S10) corroborate the insight drawn by Farfan and Turner from simulations of absorptive 2DES spectra in the presence of interfering vibronic modes. Building upon this work, we observe that the mapping of the high frequency 1350 cm⁻¹ mode onto the beatmap of the low-frequency 550 cm⁻¹ vibration persists and is significantly more evident in the rephasing beatmaps. Moreover, the shift in the fundamental vibrational frequencies from 550 to 533 cm⁻¹ and 1350 to 1367 cm⁻¹ in the single- and multiple-DHO simulations, respectively, supports the presence of an interaction between the 550 and 1350 cm⁻¹ modes.

In addition to modulating the shape of quantum beatmaps, interference between vibrational wavepackets is also predicted to generate combination bands in the power spectra of the quantum beats in 2DES.⁷⁰ As noted from Figures 3a and S7, the peak near 800 cm⁻¹ in the power spectrum for TDI is neither accounted for in the FSRS results nor the computed resonance-Raman spectrum. Figure 5a compares the experimental power spectrum to those obtained from both the single- and multiple-DHO simulations. As expected, both simulations predict beating signatures at the fundamental frequencies of the DHO(s) included. However, only the multiple-DHO simulation produces a feature near 850 cm⁻¹, which matches well with the experiment and is assigned to a difference-frequency band originating from coupling between the 550 and 1350 cm⁻¹ wavepackets. Moreover, we find reasonable agreement between the experimental and simulated beatmaps for this difference-frequency band, as shown in Figure S18. Figure 5b illustrates an example double-sided Feynman diagram that can explain quantum beats with a frequency equivalent to the frequency difference between two arbitrary vibrations α and β , in this case 550 and 1350 cm⁻¹, respectively. Importantly, such a beat frequency can only be generated by electronic excited-state evolution of the density matrix. While vibrational coherence on an excited electronic state can manifest in FSRS spectra by means of vertical-FSRS pathways, 101,102 the lack of the 800 cm⁻¹ feature in our measured FSR spectrum (Figure 3a) suggests that the groundstate FSRS signals are dominant. FSRS measurements with an actinic pump may provide further information as combination bands have been observed in this manner previously.⁹¹

For the signal pathway illustrated in Figure 5b to be observable via 2DES, vibrations α and β must not be orthogonal in the eigenstate basis. This nonorthogonality is also required to explain how the 1350 cm⁻¹ motion impacts the beatmaps for the 550 cm⁻¹ vibration. The direct experimental and theoretical comparisons put forth in Figures 4 and 5 illustrate the accuracy of the multiple-DHO model in predicting the behavior of experimental quantum beating signatures from TDI. We can therefore use this model to rationalize the physical origin of the coupling between the 550 and 1350 cm⁻¹ vibrations. Specifically, because we formulate our model with vibrations treated within the system Hamiltonian, we can pinpoint the origin of the coupling to system-specific properties. Both anharmonic coupling and the Duschinsky rotation (where the normal modes of the ground and excited electronic states are different yet related by linear combination) can induce mixing between vibrational modes. 52,69,103,104 These effects are expensive to treat in comparison to simple parallel harmonic potentials. In contrast to recent experimental reports of deviations from single-DHO

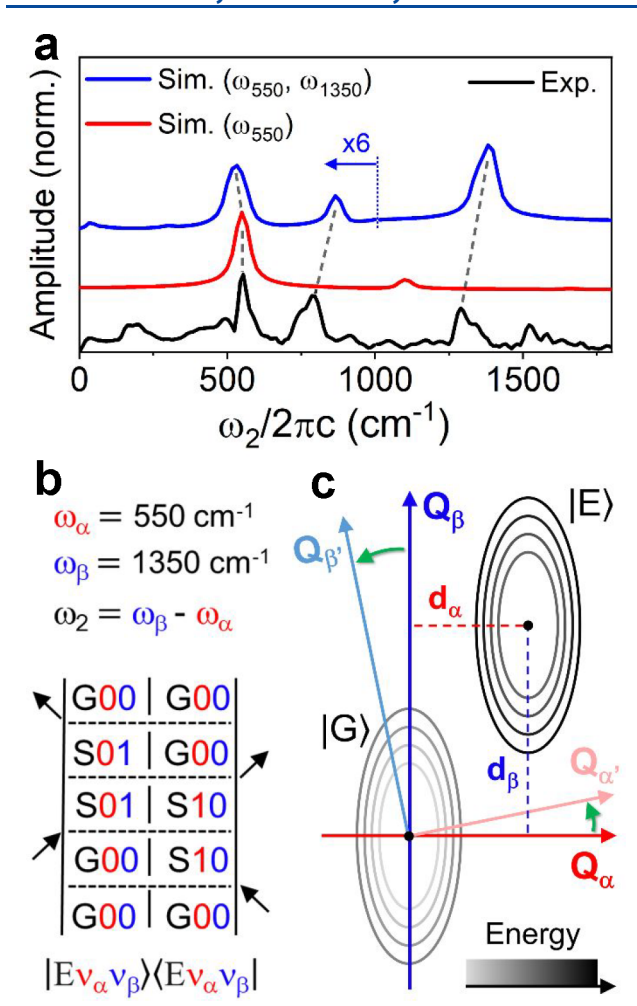


Figure 5. (a) Comparisons of experimental and simulated power spectra using both the single- and multiple-DHO Hamiltonians, (b) an example double-sided Feynman diagram that yields difference-frequency beating during t_2 , and (c) a schematic illustrating the ground- (G) and excited-state (E) potential energy surfaces for the multiple-DHO model with vibrations α and β . The diagrams in panels b and c are color coded with red and blue signifying the 550 and 1350 cm⁻¹ vibrational coordinates, respectively. Q_β (Q_α) and d_β (d_α) in panel c represent the site-basis nuclear coordinate and displacement for the β (α) vibrations, respectively, while $Q_{\beta'}$ and $Q_{\alpha'}$ indicate nuclear coordinates in the eigenstate basis. Green arrows portray the basis rotation.

beatmap predictions due to anharmonic coupling between vibrational wavepackets, 55 we find that the experimental TDI beatmaps are excellently reproduced within the harmonic approximation. Moreover, since we do not explicitly couple the vibrations in our multiple-DHO Hamiltonian, our model achieves this accuracy without accounting for a possible Duschinsky rotation. Instead, we suggest that the vibrational coupling evidenced by the TDI quantum beating signatures originates from purely harmonic coupling, similar to that used recently in the calculation of crosspeaks in two-dimensional impulsively stimulated resonant Raman spectra. 69

Figure 5c illustrates a top-down view of the potential energy surface (PES) captured by our model in the *site basis*. Importantly, the harmonic potentials for the ground-(G) and excited-(E) electronic surfaces are shaped by two orthogonal nuclear coordinates Q_{α} and Q_{β} . For TDI, where $\omega_{\alpha} = 550$ cm⁻¹ and $\omega_{\beta} = 1350$ cm⁻¹, the potentials have an elliptical

curvature since $\omega_{\alpha} \neq \omega_{\beta}$. However, the theory and its predictions are still applicable to the case where $\omega_{\alpha} = \omega_{\beta}$. Though no coupling is explicitly defined between the normal modes α and β , the PES is displaced along both nuclear coordinates by their respective HR factors. Diagonalizing the Hamiltonian to the system eigenstate basis effectively rotates the axes in Figure 5c, as shown by the green arrows, thereby yielding vibrations α' and β' , which are both linear combinations of vibrations α and β . Qualitatively, this means that treatment of multiple DHOs within the same system Hamiltonian results in purely harmonic coupling between the orthogonal vibrations, α and β in this example, which is then manifested in experimental measurements of the system eigenstates (quantum beatmaps and Fourier power spectra). We note that this interpretation has broad implications for the studies of a wide range of materials since the harmonic coupling is sensitive to the Huang-Rhys factors of all displaced oscillators within the system. Since FC activity is the only prerequisite, the effects of this harmonic coupling may manifest in 2DES experiments of individual molecules and multichromophoric systems, where the complexity of the effects will scale with both the size of the individual molecules as well as the extent of interactions within a molecular ensemble. We hypothesize that the effects of this harmonic coupling are distinct from those that would arise from direct treatment of anharmonic coupling or a Duschinsky rotation in our multiple-DHO model. While anharmonicity may play a role in shaping features in 2DES beatmaps,⁵⁵ the agreement between our simulated and experimental TDI beatmaps (Figures 4 and S10) suggests that harmonic vibrational coupling is predominantly responsible for the deviations from the predictions of the single-DHO approximation.

Generality and Implications of Coupled Vibrational Wavepackets. Taking recent studies of multicomponent vibrational wavepackets^{SS,S8,70,10S,106} in conjunction with the agreements that we observe between the multiple-DHO simulations and experimental TDI data, we posit that the single-DHO approximation breaks down more often than is commonly anticipated. Indeed, examination of the quantum beatmaps obtained in our previous study of perylenediimide-based monomers and dimers reveals that signatures of coupled vibrational and/or vibronic wavepackets are evident.⁷⁹ To further test the generality of the multiple-DHO formalism, we performed additional 2DES experiments on NB and MB, which are dye molecules applied in numerous biomedical contexts,⁷⁷ as well as ITIC, an efficient nonfullerene electron acceptor commonly employed in organic photovoltaic research.⁷⁴

Figure 6 illustrates rephasing quantum beatmaps for the oscillations near 440, 461, and 600 cm⁻¹ for MB, ITIC, and NB, respectively. We analyze the positive-signed beat frequency for each compound since, under the standard single-DHO approximation, only excited-state vibrational wavepackets modulate the positive-signed regime of the rephasing beating signals (*vide infra*). This portion of the 2DES signal is therefore of significant importance when diagnosing quantum beating signatures in complex chemical systems.

The frequencies of these beating signatures match well with that in the existing literature for MB, TITIC, S,107 and NB, 108,109 and in each case are among the strongest low-frequency vibrations coupled to their respective $S_1 \leftarrow S_0$ transitions. In each compound, the most intense quantum

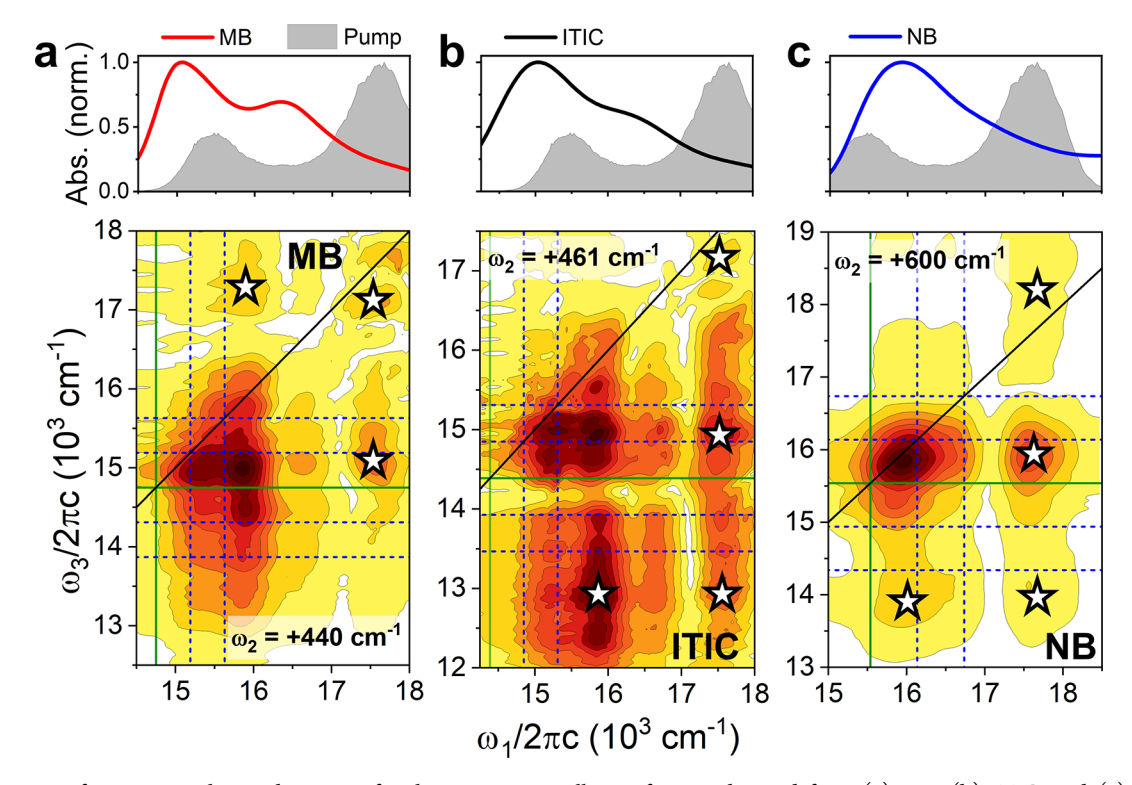


Figure 6. Positive frequency rephasing beatmaps for the strongest oscillatory feature observed from (a) MB, (b) ITIC, and (c) NB. Linear absorption spectra (solid lines) for each compound are shown in the top row with the pump spectrum (shaded gray) superimposed. The solid green lines indicate the approximate 0–0 singlet electronic transition energies, while dashed lines show energies that represent either one or two frequency quanta away from the 0–0 electronic transition energy in either the pump (vertical lines) or probe (horizontal lines) axis. Stars highlight particularly strong features that are captured well when accounting for coupling of the fundamental vibration to one or more high-frequency oscillators.

beating occurs within the region near the diagonal characteristic of a purely vibrational coherence, 53 accounting for systematic blueshifts from the $S_1 \leftarrow S_0$ transition energies^{76,109,110} due to the overlap of the molecular absorption and pump spectra. However, as denoted by the stars, numerous features in each beatmap have clear deviations from the single-DHO model (top of Figure 4c), several of which are predicted by our multiple-DHO TDI simulations (top of Figure 4d) after taking the differences in beat frequencies into consideration. We expect that thorough accounting for the number, frequencies, and HR factors of the FC-active modes in each of these compounds would yield better agreement between simulation and experiment. These findings illustrate the general applicability of the multiple-DHO model and the importance of accounting for multiple nuclear coordinates when rationalizing quantum beating signatures in 2DES data.

In numerous previous works, positive-frequency quantum beats in the rephasing 2DES signal have been utilized to study purely excited-state wavepacket evolution, often for the purpose of connecting a particular vibrational mode to a reaction coordinate. Figure 7a shows a simulated TDI beatmap from the rephasing GSB response function (eq S7) using the single- DHO Hamiltonian. The maximum amplitude in the simulated $\omega_2 = -550$ cm⁻¹ beatmap, located in the diagonal feature near $\omega_1 = \omega_3 = 15300$ cm⁻¹, is nearly 90 times stronger than that of the $\omega_2 = +550$ cm⁻¹ beatmap. This result matches the expectation that ground-state wavepackets minimally modulate rephasing beatmaps for positive ω_2 values. However, we find that the multiple-DHO model, including

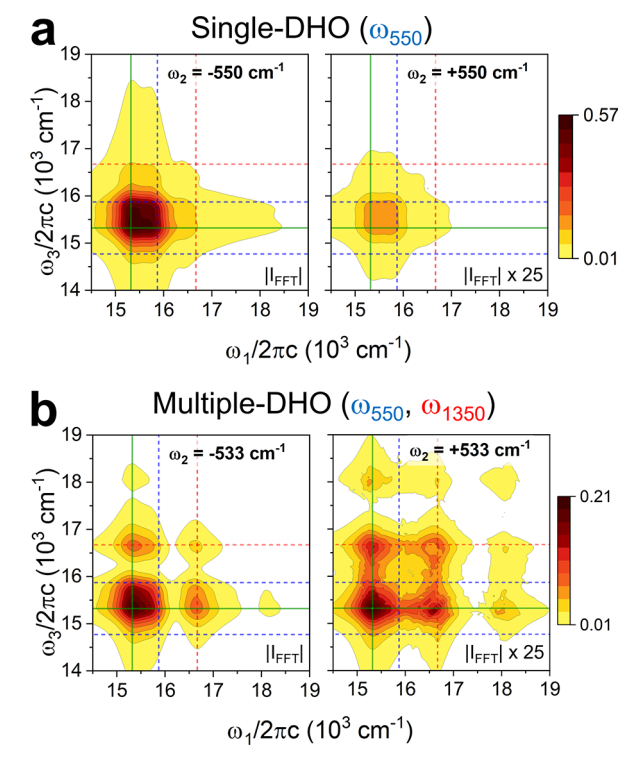


Figure 7. Simulated rephasing-GSB quantum beatmaps for the (a) single-DHO and (b) multiple-DHO models parametrized for TDI. The quantum beating signatures are partitioned into positive and negative ω_2 amplitudes.

both 550 and 1350 cm⁻¹ vibrations, reveals a fallacy in this assumption, as shown in Figure 7b. In this case, the maximum amplitude of the $\omega_2 = +533$ cm⁻¹ oscillation relative to that of the $\omega_2 = -533$ cm⁻¹ frequency increases 350% in comparison to the corresponding relative maximum amplitude from the single-DHO simulation. Moreover, coupling between the lowand high-frequency wavepackets is particularly evident as a new diagonal feature and corresponding crosspeaks aligned with vertical transition energies corresponding to the 1350 cm⁻¹ mode appear.

Figure 7 illustrates that including more than one DHO when examining vibrational wavepackets with 2DES and quantum beatmaps may lead to the breakdown of common assumptions, such as neglecting the ground-state background in positively signed rephasing beatmaps. More generally, dressing Holsteinlike Hamiltonians with additional vibrations will invoke nontrivial deviations from the conventional beatmaps predicted under the single-DHO approximation. We anticipate the effects of coupled harmonic wavepacket evolution will be even more pronounced and complex in studies of interacting, multichromophoric systems. This would imply that established approaches for disentangling signatures of vibrational, vibronic, and/or electronic coherence from the quantum beatmaps of molecular aggregates may be perturbed when the FC envelope consists of numerous vibrations. However, we believe this framework may help elucidate the nature of photochemical reactions that are driven by an interplay of vibrations and, in turn, increase the accuracy of molecular design rules that are informed by 2DES experiments. Future work aims to expand these multiple-DHO simulations to molecular aggregates and critically assess these hypotheses. Though addressing numerous nuclear dimensions intensifies the required computational resources, the multiple-DHO model that we employed here requires relatively little input and can be applied in advance of 2DES experimentation. For example, experimental or computed steady-state absorption and resonance Raman spectra for a monomeric chromophore is sufficient to parametrize the multiple-DHO Hamiltonian and guide further experimental design.

CONCLUSIONS

We examined coupling between vibrational wavepackets in both theoretical and experimental contexts. Direct comparison of simulations using the single- and multiple-DHO Hamiltonians shows clear evidence for the substantial effects of such coupling in the experimental 2DES quantum beating signatures collected from TDI, ITIC, MB, and NB. We experimentally and theoretically demonstrated that harmonic coupling between vibrational wavepackets results in nontrivial mixing of their respective quantum beatmaps. We attribute this effect to the fact that both DHOs in our multiple-DHO simulations are treated simultaneously and on equal footing, which results in coupling between the originally orthogonal site-basis vibrations, even in the absence of anharmonic interactions. We note that this situation is applicable to any molecular system with two or more FC-active vibrations. We showed that the multiple-DHO model reveals the breakdown of the assumption that positive rephasing beat frequencies correspond to vibrational wavepacket motion solely in the electronically excited manifold of an isolated chromophore. This represents a clear instance in which the single-DHO model may misdirect the translation of quantum beatmaps into meaningful chemical insight, particularly in studies of complex,

multichromophoric systems. Considering that 2DES beatmaps are a current and vital tool for interrogating the potential energy landscape of key photodriven reactions, we stress the importance of accounting for the possible observables that can originate from coupled nuclear degrees of freedom in these experiments.

ASSOCIATED CONTENT

Supporting Information

The Supporting Information is available free of charge at https://pubs.acs.org/doi/10.1021/acs.jpcc.1c09432.

Additional details for methods and instrumentation, data analysis, additional and replicate 2DES spectra, power spectra, quantum beatmaps, and simulations (PDF)

AUTHOR INFORMATION

Corresponding Author

Michael R. Wasielewski — Department of Chemistry and Institute for Sustainability and Energy at Northwestern, Northwestern University, Evanston, Illinois 60208-3113, United States; orcid.org/0000-0003-2920-5440; Email: m-wasielewski@northwestern.edu

Authors

Jonathan D. Schultz – Department of Chemistry and Institute for Sustainability and Energy at Northwestern, Northwestern University, Evanston, Illinois 60208-3113, United States; orcid.org/0000-0002-3386-5460

Taeyeon Kim — Department of Chemistry and Institute for Sustainability and Energy at Northwestern, Northwestern University, Evanston, Illinois 60208-3113, United States; orcid.org/0000-0003-0408-9498

James P. O'Connor – Department of Chemistry and Institute for Sustainability and Energy at Northwestern, Northwestern University, Evanston, Illinois 60208-3113, United States; orcid.org/0000-0002-8586-9842

Ryan M. Young — Department of Chemistry and Institute for Sustainability and Energy at Northwestern, Northwestern University, Evanston, Illinois 60208-3113, United States; orcid.org/0000-0002-5108-0261

Complete contact information is available at: https://pubs.acs.org/10.1021/acs.jpcc.1c09432

Notes

The authors declare no competing financial interest. The data discussed in this work and the codes used to process them are available from the authors upon reasonable request.

ACKNOWLEDGMENTS

We thank Professor Roel Tempelaar and Professor Jae Yoon Shin for insightful discussions pertaining to the simulations and experimental comparisons conducted for this work, Dr. Itai Schlesinger for fruitful conversations regarding the physical interpretation of harmonic coupling, Dr. Xingang Zhao and Dr. Michelle Chen for synthesizing TDI, and Gyeongwon Kang, Dr. Leighton Jones, and Professor Martin Mosquera for helpful discussions regarding resonance Raman DFT computations with the ADF software package. This work was supported by the National Science Foundation under Award CHE-1925690 (M.R.W.). This material is based upon work supported by the National Science Foundation Graduate Research Fellowship Program under Grant No. DGE-1842165 (J.D.S.). Any

opinions, findings, and conclusions or recommendations expressed in this material are those of the author(s) and do not necessarily reflect the views of the National Science Foundation.

REFERENCES

- (1) Scholes, G. D.; Fleming, G. R.; Chen, L. X.; Aspuru-Guzik, A.; Buchleitner, A.; Coker, D. F.; Engel, G. S.; van Grondelle, R.; Ishizaki, A.; Jonas, D. M.; et al. Using coherence to enhance function in chemical and biophysical systems. *Nature* **2017**, *543*, 647–656.
- (2) Collini, E.; Gattuso, H.; Bolzonello, L.; Casotto, A.; Volpato, A.; Dibenedetto, C. N.; Fanizza, E.; Striccoli, M.; Remacle, F. Quantum phenomena in nanomaterials: Coherent superpositions of fine structure states in CdSe nanocrystals at room temperature. *J. Phys. Chem. C* 2019, 123, 31286–31293.
- (3) Collini, E. 2D electronic spectroscopic techniques for quantum technology applications. *J. Phys. Chem. C* **2021**, *125*, 13096–13108.
- (4) Pandya, R.; Chen, R. Y. S.; Cheminal, A.; Thomas, T.; Thampi, A.; Tanoh, A.; Richter, J.; Shivanna, R.; Deschler, F.; Schnedermann, C.; et al. Observation of vibronic-coupling-mediated energy transfer in light-harvesting nanotubes stabilized in a solid-state matrix. *J. Phys. Chem. Lett.* **2018**, *9*, 5604–5611.
- (5) Womick, J. M.; Moran, A. M. Vibronic enhancement of exciton sizes and energy transport in photosynthetic complexes. *J. Phys. Chem. B* **2011**, *115*, 1347–1356.
- (6) Dean, J. C.; Mirkovic, T.; Toa, Z. S. D.; Oblinsky, D. G.; Scholes, G. D. Vibronic enhancement of algae light harvesting. *Chem.* **2016**, *1*, 858–872.
- (7) Kim, J.; Nguyen-Phan, T. C.; Gardiner, A. T.; Cogdell, R. J.; Scholes, G. D.; Cho, M. Low-frequency vibronic mixing modulates the excitation energy flow in bacterial light-harvesting complex II. *J. Phys. Chem. Lett.* **2021**, *12*, 6292–6298.
- (8) Lewis, K. L. M.; Ogilvie, J. P. Probing photosynthetic energy and charge transfer with two-dimensional electronic spectroscopy. *J. Phys. Chem. Lett.* **2012**, *3*, 503–510.
- (9) Perlík, V.; Seibt, J.; Cranston, L. J.; Cogdell, R. J.; Lincoln, C. N.; Savolainen, J.; Šanda, F.; Mančal, T.; Hauer, J. Vibronic coupling explains the ultrafast carotenoid-to-bacteriochlorophyll energy transfer in natural and artificial light harvesters. *J. Chem. Phys.* **2015**, *142*, 212434.
- (10) Irgen-Gioro, S.; Gururangan, K.; Spencer, A. P.; Harel, E. Non-uniform excited state electronic-vibrational coupling of pigment—protein complexes. *J. Phys. Chem. Lett.* **2020**, *11*, 10388–10395.
- (11) Falke, S. M.; Rozzi, C. A.; Brida, D.; Maiuri, M.; Amato, M.; Sommer, E.; De Sio, A.; Rubio, A.; Cerullo, G.; Molinari, E.; Lienau, C. Coherent ultrafast charge transfer in an organic photovoltaic blend. *Science* **2014**, *344*, 1001–1005.
- (12) Andrea Rozzi, C.; Maria Falke, S.; Spallanzani, N.; Rubio, A.; Molinari, E.; Brida, D.; Maiuri, M.; Cerullo, G.; Schramm, H.; Christoffers, J.; Lienau, C. Quantum coherence controls the charge separation in a prototypical artificial light-harvesting system. *Nat. Commun.* **2013**, *4*, 1602.
- (13) Rafiq, S.; Scholes, G. D. Is back-electron transfer process in betaine-30 coherent? *Chem. Phys. Lett.* **2017**, *683*, 500–506.
- (14) Rafiq, S.; Fu, B.; Kudisch, B.; Scholes, G. D. Interplay of vibrational wavepackets during an ultrafast electron transfer reaction. *Nat. Chem.* **2021**, *13*, 70–76.
- (15) Song, Y.; Clafton, S. N.; Pensack, R. D.; Kee, T. W.; Scholes, G. D. Vibrational coherence probes the mechanism of ultrafast electron transfer in polymer–fullerene blends. *Nat. Commun.* **2014**, *5*, 4933.
- (16) De Sio, A.; Lienau, C. Vibronic coupling in organic semiconductors for photovoltaics. *Phys. Chem. Chem. Phys.* **2017**, 19, 18813–18830.
- (17) Rafiq, S.; Scholes, G. D. From fundamental theories to quantum coherences in electron transfer. *J. Am. Chem. Soc.* **2019**, *141*, 708–722.
- (18) Kim, P.; Valentine, A. J. S.; Roy, S.; Mills, A. W.; Chakraborty, A.; Castellano, F. N.; Li, X.; Chen, L. X. Ultrafast excited-state

- dynamics of photoluminescent Pt(II) dimers probed by a coherent vibrational wavepacket. *J. Phys. Chem. Lett.* **2021**, *12*, 6794–6803.
- (19) Kim, T.; Kim, W.; Vakuliuk, O.; Gryko, D. T.; Kim, D. Two-step charge separation passing through the partial charge-transfer state in a molecular dyad. *J. Am. Chem. Soc.* **2020**, *142*, 1564–1573.
- (20) Kim, W.; Kim, T.; Kang, S.; Hong, Y.; Würthner, F.; Kim, D. Tracking structural evolution during symmetry-breaking charge separation in quadrupolar perylene bisimide with time-resolved impulsive stimulated raman spectroscopy. *Angew. Chem., Int. Ed.* **2020**, *132*, 8649–8656.
- (21) Yoneda, Y.; Mora, S. J.; Shee, J.; Wadsworth, B. L.; Arsenault, E. A.; Hait, D.; Kodis, G.; Gust, D.; Moore, G. F.; Moore, A. L.; et al. Electron–nuclear dynamics accompanying proton-coupled electron transfer. *J. Am. Chem. Soc.* **2021**, *143*, 3104–3112.
- (22) Fuller, F. D.; Pan, J.; Gelzinis, A.; Butkus, V.; Senlik, S. S.; Wilcox, D. E.; Yocum, C. F.; Valkunas, L.; Abramavicius, D.; Ogilvie, J. P. Vibronic coherence in oxygenic photosynthesis. *Nat. Chem.* **2014**, 6, 706–711.
- (23) Schultz, J. D.; Shin, J. Y.; Chen, M.; O'Connor, J. P.; Young, R. M.; Ratner, M. A.; Wasielewski, M. R. Influence of vibronic coupling on ultrafast singlet fission in a linear terrylenediimide dimer. *J. Am. Chem. Soc.* **2021**, *143*, 2049–2058.
- (24) Monahan, N. R.; Sun, D.; Tamura, H.; Williams, K. W.; Xu, B.; Zhong, Y.; Kumar, B.; Nuckolls, C.; Harutyunyan, A. R.; Chen, G.; et al. Dynamics of the triplet-pair state reveals the likely coexistence of coherent and incoherent singlet fission in crystalline hexacene. *Nat. Chem.* **2017**, *9*, 341–346.
- (25) Bakulin, A. A.; Morgan, S. E.; Kehoe, T. B.; Wilson, M. W. B.; Chin, A. W.; Zigmantas, D.; Egorova, D.; Rao, A. Real-time observation of multiexcitonic states in ultrafast singlet fission using coherent 2D electronic spectroscopy. *Nat. Chem.* **2016**, *8*, 16–23.
- (26) Duan, H.-G.; Jha, A.; Li, X.; Tiwari, V.; Ye, H.; Nayak, P. K.; Zhu, X.-L.; Li, Z.; Martinez, T. J.; Thorwart, M.; Miller, R. J. D. Intermolecular vibrations mediate ultrafast singlet fission. *Sci. Adv.* **2020**, *6*, eabb0052.
- (27) Miyata, K.; Kurashige, Y.; Watanabe, K.; Sugimoto, T.; Takahashi, S.; Tanaka, S.; Takeya, J.; Yanai, T.; Matsumoto, Y. Coherent singlet fission activated by symmetry breaking. *Nat. Chem.* **2017**, *9*, 983–989.
- (28) Wang, G.; Zhang, C.; Liu, Z.; Wang, R.; Ma, H.; Wang, X.; Xiao, M. Singlet fission dynamics in tetracene single crystals probed by polarization-dependent two-dimensional electronic spectroscopy. *J. Phys. Chem. A* **2020**, *124*, 10447–10456.
- (29) Alvertis, A. M.; Lukman, S.; Hele, T. J. H.; Fuemmeler, E. G.; Feng, J.; Wu, J.; Greenham, N. C.; Chin, A. W.; Musser, A. J. Switching between coherent and incoherent singlet fission via solvent-induced symmetry breaking. *J. Am. Chem. Soc.* **2019**, *141*, 17558–17570
- (30) Kang, S.; Kim, T.; Hong, Y.; Würthner, F.; Kim, D. Charge-delocalized state and coherent vibrational dynamics in rigid PBI Haggregates. *J. Am. Chem. Soc.* **2021**, *143*, 9825–9833.
- (31) Kim, T.; Kang, S.; Kirchner, E.; Bialas, D.; Kim, W.; Würthner, F.; Kim, D. Switching resonance character within merocyanine stacks and its impact on excited-state dynamics. *Chem.* **2021**, *7*, 715–725.
- (32) Christopher, R.; Frontiera, R. R. Coherent phonon catalysts: Lattice vibrations drive a photoinduced phase transition in a molecular crystal. *J. Phys. Chem. Lett.* **2021**, *11*, 7502–7509.
- (33) Horstmann, J. G.; Böckmann, H.; Wit, B.; Kurtz, F.; Storeck, G.; Ropers, C. Coherent control of a surface structural phase transition. *Nature* **2020**, *583*, 232–236.
- (34) Jumper, C. C.; Arpin, P. C.; Turner, D. B.; McClure, S. D.; Rafiq, S.; Dean, J. C.; Cina, J. A.; Kovac, P. A.; Mirkovic, T.; Scholes, G. D. Broad-band pump—probe spectroscopy quantifies ultrafast solvation dynamics of proteins and molecules. *J. Phys. Chem. Lett.* **2016**, *7*, 4722—4731.
- (35) Patra, S.; Sahu, A.; Tiwari, V. Effective normal modes identify vibrational motions which maximally promote vibronic mixing in excitonically coupled aggregates. *J. Chem. Phys.* **2021**, *154*, 111106.

- (36) Tempelaar, R.; Reichman, D. R. Vibronic exciton theory of singlet fission. II. Two-dimensional spectroscopic detection of the correlated triplet pair state. *J. Chem. Phys.* **2017**, *146*, 174704.
- (37) Lim, J.; Palecek, D.; Caycedo-Soler, F.; Lincoln, C. N.; Prior, J.; von Berlepsch, H.; Huelga, S. F.; Plenio, M. B.; Zigmantas, D.; Hauer, J. Vibronic origin of long-lived coherence in an artificial molecular light harvester. *Nat. Commun.* **2015**, *6*, 7755.
- (38) Halpin, A.; Johnson, P. J.; Tempelaar, R.; Murphy, R. S.; Knoester, J.; Jansen, T. L.; Miller, R. J. Two-dimensional spectroscopy of a molecular dimer unveils the effects of vibronic coupling on exciton coherences. *Nat. Chem.* **2014**, *6*, 196–201.
- (39) Chenu, A.; Christensson, N.; Kauffmann, H. F.; Mancal, T. Enhancement of vibronic and ground-state vibrational coherences in 2D spectra of photosynthetic complexes. *Sci. Rep.* **2013**, *3*, 2029.
- (40) Shim, S.-H.; Zanni, M. T. How to turn your pump-probe instrument into a multidimensional spectrometer: 2D IR and Vis spectroscopies via pulse shaping. *Phys. Chem. Chem. Phys.* **2009**, *11*, 748–761.
- (41) Fuller, F. D.; Ogilvie, J. P. Experimental implementations of two-dimensional Fourier transform electronic spectroscopy. *Annu. Rev. Phys. Chem.* **2015**, *66*, 667–90.
- (42) Mančal, T. A decade with quantum coherence: How our past became classical and the future turned quantum. *Chem. Phys.* **2020**, 532, 110663.
- (43) Hybl, J. D.; Albrecht Ferro, A.; Jonas, D. M. Two-dimensional Fourier transform electronic spectroscopy. *J. Chem. Phys.* **2001**, *115*, 6606
- (44) Dean, J. C.; Scholes, G. D. Coherence spectroscopy in the condensed phase: Insights into molecular structure, environment, and interactions. *Acc. Chem. Res.* **2017**, *50*, 2746–2755.
- (45) Thyrhaug, E.; Tempelaar, R.; Alcocer, M. J. P.; Zidek, K.; Bina, D.; Knoester, J.; Jansen, T. L. C.; Zigmantas, D. Identification and characterization of diverse coherences in the Fenna-Matthews-Olson complex. *Nat. Chem.* **2018**, *10*, 780–786.
- (46) Irgen-Gioro, S.; Gururangan, K.; Saer, R. G.; Blankenship, R. E.; Harel, E. Electronic coherence lifetimes of the Fenna-Matthews-Olson complex and light harvesting complex II. *Chem. Sci.* **2019**, *10*, 10503—10509.
- (47) Song, Y.; Clafton, S. N.; Pensack, R. D.; Kee, T. W.; Scholes, G. D. Vibrational coherence probes the mechanism of ultrafast electron transfer in polymer-fullerene blends. *Nat. Commun.* **2014**, *5*, 4933.
- (48) Bredas, J. L.; Sargent, E. H.; Scholes, G. D. Photovoltaic concepts inspired by coherence effects in photosynthetic systems. *Nat. Mater.* **2017**, *16*, 35–44.
- (49) Wang, L.; Griffin, G. B.; Zhang, A.; Zhai, F.; Williams, N. E.; Jordan, R. F.; Engel, G. S. Controlling quantum-beating signals in 2D electronic spectra by packing synthetic heterodimers on single-walled carbon nanotubes. *Nat. Chem.* **2017**, *9*, 219–225.
- (50) Hart, S. M.; Chen, W. J.; Banal, J. L.; Bricker, W. P.; Dodin, A.; Markova, L.; Vyborna, Y.; Willard, A. P.; Häner, R.; Bathe, M.; et al. Engineering couplings for exciton transport using synthetic DNA scaffolds. *Chem.* **2021**, *7*, 752–773.
- (51) Milota, F.; Prokhorenko, V. I.; Mancal, T.; Von Berlepsch, H.; Bixner, O.; Kauffmann, H. F.; Hauer, J. Vibronic and vibrational coherences in two-dimensional electronic spectra of supramolecular Jaggregates. *J. Phys. Chem. A* **2013**, *117*, 6007–6014.
- (52) Arpin, P. C.; Turner, D. B. Signatures of vibrational and electronic quantum beats in femtosecond coherence spectra. *J. Phys. Chem. A* **2021**, *125*, 2425–2435.
- (53) Butkus, V.; Zigmantas, D.; Valkunas, L.; Abramavicius, D. Vibrational vs. Electronic coherences in 2D spectrum of molecular systems. *Chem. Phys. Lett.* **2012**, *545*, 40–43.
- (54) Le, D. V.; Leng, X.; Tan, H.-S. Regarding expressions of the oscillatory patterns in the 2D spectra of a displaced oscillator model. *Chem. Phys.* **2021**, 546, 111142.
- (55) Zhu, R.; Zou, J.; Wang, Z.; Chen, H.; Weng, Y. Electronic stateresolved multimode-coupled vibrational wavepackets in oxazine 720 by two-dimensional electronic spectroscopy. *J. Phys. Chem. A* **2020**, 124, 9333–9342.

- (56) Hart, S. M.; Banal, J. L.; Bathe, M.; Schlau-Cohen, G. S. Identification of nonradiative decay pathways in cy3. *J. Phys. Chem. Lett.* **2020**, *11*, 5000–5007.
- (57) Kuramochi, H.; Tahara, T. Tracking ultrafast structural dynamics by time-domain raman spectroscopy. *J. Am. Chem. Soc.* **2021**, *143*, 9699–9717.
- (58) Yue, S.; Wang, Z.; Leng, X.; Zhu, R. D.; Chen, H. L.; Weng, Y. X. Coupling of multi-vibrational modes in bacteriochlorophyll a in solution observed with 2D electronic spectroscopy. *Chem. Phys. Lett.* **2017**, *683*, 591–597.
- (59) Le, D. V.; De La Perrelle, J. M.; Do, T. N.; Leng, X.; Tapping, P. C.; Scholes, G. D.; Kee, T. W.; Tan, H.-S. Characterization of the ultrafast spectral diffusion and vibronic coherence of tips-pentacene using 2D electronic spectroscopy. *J. Chem. Phys.* **2021**, *155*, 014302.
- (60) Hamm, P.; Lim, M.; Hochstrasser, R. M. Structure of the amide I band of peptides measured by femtosecond nonlinear-infrared spectroscopy. *J. Phys. Chem. B* **1998**, *102*, 6123–6138.
- (61) Zanni, M. T.; Hochstrasser, R. M. Two-dimensional infrared spectroscopy: A promising new method for the time resolution of structures. *Curr. Opin. Struct. Biol.* **2001**, *11*, 516–522.
- (62) Gaynor, J. D.; Weakly, R. B.; Khalil, M. Multimode two-dimensional vibronic spectroscopy. I. Orientational response and polarization-selectivity. *J. Chem. Phys.* **2021**, *154*, 184201.
- (63) Weakly, R. B.; Gaynor, J. D.; Khalil, M. Multimode twodimensional vibronic spectroscopy. II. Simulating and extracting vibronic coupling parameters from polarization-selective spectra. *J. Chem. Phys.* **2021**, *154*, 184202.
- (64) Gaynor, J. D.; Sandwisch, J.; Khalil, M. Vibronic coherence evolution in multidimensional ultrafast photochemical processes. *Nat. Commun.* **2019**, *10*, 5621.
- (65) Arsenault, E. A.; Yoneda, Y.; Iwai, M.; Niyogi, K. K.; Fleming, G. R. Vibronic mixing enables ultrafast energy flow in light-harvesting complex II. *Nat. Commun.* **2020**, *11*, 1460.
- (66) Arsenault, E. A.; Bhattacharyya, P.; Yoneda, Y.; Fleming, G. R. Two-dimensional electronic—vibrational spectroscopy: Exploring the interplay of electrons and nuclei in excited state molecular dynamics. *J. Chem. Phys.* **2021**, *155*, 020901.
- (67) Arsenault, E. A.; Schile, A. J.; Limmer, D. T.; Fleming, G. R. Vibronic coupling in energy transfer dynamics and two-dimensional electronic—vibrational spectra. *J. Chem. Phys.* **2021**, *155*, 054201.
- (68) Fox, Z. W.; Blair, T. J.; Khalil, M. Determining the orientation and vibronic couplings between electronic and vibrational coordinates with polarization-selective two-dimensional vibrational-electronic spectroscopy. *J. Phys. Chem. Lett.* **2020**, *11*, 1558–1563.
- (69) Fumero, G.; Schnedermann, C.; Batignani, G.; Wende, T.; Liebel, M.; Bassolino, G.; Ferrante, C.; Mukamel, S.; Kukura, P.; Scopigno, T. Two-dimensional impulsively stimulated resonant raman spectroscopy of molecular excited states. *Phys. Rev. X* **2020**, *10*, 011051.
- (70) Farfan, C. A.; Turner, D. B. Interference among multiple vibronic modes in two-dimensional electronic spectroscopy. *Mathematics* **2020**, *8*, 157.
- (71) Zhan, X.; Facchetti, A.; Barlow, S.; Marks, T. J.; Ratner, M. A.; Wasielewski, M. R.; Marder, S. R. Rylene and related diimides for organic electronics. *Adv. Mater.* **2011**, *23*, 268–284.
- (72) Margulies, E. A.; Kerisit, N.; Gawel, P.; Mauck, C. M.; Ma, L.; Miller, C. E.; Young, R. M.; Trapp, N.; Wu, Y. L.; Diederich, F.; et al. Substituent effects on singlet exciton fission in polycrystalline thin films of cyano-substituted diaryltetracenes. *J. Phys. Chem. C* **2017**, 121, 21262–21271.
- (73) Margulies, E. A.; Miller, C. E.; Wu, Y.; Ma, L.; Schatz, G. C.; Young, R. M.; Wasielewski, M. R. Enabling singlet fission by controlling intramolecular charge transfer in π -stacked covalent terrylenediimide dimers. *Nat. Chem.* **2016**, *8*, 1120–1125.
- (74) Eastham, N. D.; Logsdon, J. L.; Manley, E. F.; Aldrich, T. J.; Leonardi, M. J.; Wang, G.; Powers-Riggs, N. E.; Young, R. M.; Chen, L. X.; Wasielewski, M. R.; et al. Hole-transfer dependence on blend morphology and energy level alignment in polymer: ITIC photovoltaic materials. *Adv. Mater.* **2018**, *30*, 1704263.

- (75) Song, Y.; Liu, X.; Li, Y.; Nguyen, H. H.; Duan, R.; Kubarych, K. J.; Forrest, S. R.; Ogilvie, J. P. Mechanistic study of charge separation in a nonfullerene organic donor—acceptor blend using multispectral multidimensional spectroscopy. *J. Phys. Chem. Lett.* **2021**, *12*, 3410—3416.
- (76) Dean, J. C.; Oblinsky, D. G.; Rafiq, S.; Scholes, G. D. Methylene blue exciton states steer nonradiative relaxation: Ultrafast spectroscopy of methylene blue dimer. *J. Phys. Chem. B* **2016**, *120*, 440–454.
- (77) Dean, J. C.; Rafiq, S.; Oblinsky, D. G.; Cassette, E.; Jumper, C. C.; Scholes, G. D. Broadband transient absorption and two-dimensional electronic spectroscopy of methylene blue. *J. Phys. Chem. A* **2015**, *119*, 9098–9108.
- (78) Mandal, A.; Chen, M.; Foszcz, E.; Schultz, J. D.; Kearns, N. M.; Young, R. M.; Zanni, M. T.; Wasielewski, M. R. Two-dimensional electronic spectroscopy reveals excitation energy-dependent state mixing during singlet fission in a terrylenediimide dimer. *J. Am. Chem. Soc.* 2018, 140, 17907–17914.
- (79) Schultz, J. D.; Coleman, A. F.; Mandal, A.; Shin, J. Y.; Ratner, M. A.; Young, R. M.; Wasielewski, M. R. Steric interactions impact vibronic and vibrational coherences in perylenediimide cyclophanes. *J. Phys. Chem. Lett.* **2019**, *10*, 7498–7504.
- (80) Jones, A. C.; Kunz, M. B.; Tigges-Green, I.; Zanni, M. T. Dual spectral phase and diffraction angle compensation of a broadband AOM 4-f pulse-shaper for ultrafast spectroscopy. *Opt. Express* **2019**, 27, 37236–37247.
- (81) Zhang, Z.; Wells, K. L.; Hyland, E. W. J.; Tan, H.-S. Phase-cycling schemes for pump-probe beam geometry two-dimensional electronic spectroscopy. *Chem. Phys. Lett.* **2012**, *550*, 156–161.
- (82) Myers, J. A.; Lewis, K. L. M.; Tekavec, P. F.; Ogilvie, J. P. Two-color two-dimensional Fourier transform electronic spectroscopy with a pulse-shaper. *Opt. Express* **2008**, *16*, 17420–17428.
- (83) Mandal, A.; Schultz, J. D.; Wu, Y.-L.; Coleman, A. F.; Young, R. M.; Wasielewski, M. R. Transient two-dimensional electronic spectroscopy: Coherent dynamics at arbitrary times along the reaction coordinate. *J. Phys. Chem. Lett.* **2019**, *10*, 3509–3515.
- (84) Kirschner, M. S.; Jeong, Y.; Spencer, A. P.; Watkins, N. E.; Lin, X.-M.; Schatz, G. C.; Chen, L. X.; Schaller, R. D. Phonon-induced plasmon-exciton coupling changes probed via oscillation-associated spectra. *Appl. Phys. Lett.* **2019**, *115*, 111903.
- (85) Brown, K. E.; Veldkamp, B. S.; Co, D. T.; Wasielewski, M. R. Vibrational dynamics of a perylene-perylenediimide donor-acceptor dyad probed with femtosecond stimulated raman spectroscopy. *J. Phys. Chem. Lett.* **2012**, *3*, 2362–2366.
- (86) Kubo, R. Fluctuation, relaxation, and resonance in magnetic systems; Oliver and Boyd: London, 1962.
- (87) Laury, M. L.; Carlson, M. J.; Wilson, A. K. Vibrational frequency scale factors for density functional theory and the polarization consistent basis sets. *J. Comput. Chem.* **2012**, 33, 2380–2387
- (88) Gelin, M. F.; Chen, L.; Borrelli, R.; Thyrhaug, E. Generalized Huang-Rhys factors for molecular aggregates. *Chem. Phys.* **2020**, *528*, 110495
- (89) de A. Camargo, F. V.; Grimmelsmann, L.; Anderson, H. L.; Meech, S. R.; Heisler, I. A. Resolving vibrational from electronic coherences in two-dimensional electronic spectroscopy: The role of the laser spectrum. *Phys. Rev. Lett.* **2017**, *118*, 033001.
- (90) Duschinsky, F. The importance of the electron spectrum in multi atomic molecules. Concerning the franck-condon principle. *Acta Physicochim. URSS* **1937**, *7*, 551–566.
- (91) Ellis, S. R.; Hoffman, D. P.; Park, M.; Mathies, R. A. Difference bands in time-resolved femtosecond stimulated raman spectra of photoexcited intermolecular electron transfer from chloronaphthalene to tetracyanoethylene. *J. Phys. Chem. A* **2018**, *122*, 3594–3605.
- (92) Jonas, D. M.; Bradforth, S. E.; Passino, S. A.; Fleming, G. R. Femtosecond wavepacket spectroscopy: Influence of temperature, wavelength, and pulse duration. *J. Phys. Chem.* **1995**, *99*, 2594–2608. (93) Cao, J.; Cogdell, R. J.; Coker, D. F.; Duan, H.-G.; Hauer, J.;

Kleinekathofer, U.; Jansen, T. L. C.; Mancal, T.; Miller, R. J. D.;

- Ogilvie, J. P.; Prokhorenko, V. I.; Renger, T.; Tan, H.-S.; Tempelaar, R.; Thorwart, M.; Thyrhaug, E.; Westenhoff, S.; Zigmantas, D. Quantum biology revisited. *Sci. Adv.* **2020**, *6*, eaaz4888.
- (94) Fitzpatrick, C.; Odhner, J. H.; Levis, R. J. Spectral signatures of ground- and excited-state wavepacket interference after impulsive excitation. *J. Phys. Chem. A* **2020**, *124*, 6856–6866.
- (95) Perlík, V.; Lincoln, C.; Šanda, F.; Hauer, J. Distinguishing electronic and vibronic coherence in 2D spectra by their temperature dependence. *J. Phys. Chem. Lett.* **2014**, *5*, 404–407.
- (96) Song, Y.; Hellmann, C.; Stingelin, N.; Scholes, G. D. The separation of vibrational coherence from ground- and excited-electronic states in P3HT film. *J. Chem. Phys.* **2015**, *142*, 212410.
- (97) Volpato, A.; Bolzonello, L.; Meneghin, E.; Collini, E. Global analysis of coherence and population dynamics in 2d electronic spectroscopy. *Opt. Express* **2016**, *24*, 24773.
- (98) Paleček, D.; Edlund, P.; Westenhoff, S.; Zigmantas, D. Quantum coherence as a witness of vibronically hot energy transfer in bacterial reaction center. *Sci. Adv.* **2017**, *3*, e1603141.
- (99) Turner, D. B.; Arpin, P. C. Basis set truncation further clarifies vibrational coherence spectra. *Chem. Phys.* **2020**, *539*, 110948.
- (100) Tiwari, V.; Peters, W. K.; Jonas, D. M. Electronic resonance with anticorrelated pigment vibrations drives photosynthetic energy transfer outside the adiabatic framework. *Proc. Natl. Acad. Sci. U. S. A.* **2013**, *110*, 1203–1208.
- (101) Quick, M.; Dobryakov, A. L.; Kovalenko, S. A.; Ernsting, N. P. Resonance femtosecond-stimulated raman spectroscopy without actinic excitation showing low-frequency vibrational activity in the S_2 state of all-trans β -carotene. *J. Phys. Chem. Lett.* **2015**, *6*, 1216–1220.
- (102) Dobryakov, A. L.; Quick, M.; Ioffe, I. N.; Granovsky, A. A.; Ernsting, N. P.; Kovalenko, S. A. Excited-state raman spectroscopy with and without actinic excitation: S_1 raman spectra of transazobenzene. *J. Chem. Phys.* **2014**, *140*, 184310.
- (103) Fidler, A. F.; Engel, G. S. Nonlinear spectroscopic theory of displaced harmonic oscillators with differing curvatures: A correlation function approach. *J. Phys. Chem. A* **2013**, *117*, 9444–9453.
- (104) Zuehlsdorff, T. J.; Hong, H.; Shi, L.; Isborn, C. M. Nonlinear spectroscopy in the condensed phase: The role of Duschinsky rotations and third order cumulant contributions. *J. Chem. Phys.* **2020**, *153*, 044127.
- (105) Weng, Y. X. Detection of electronic coherence via twodimensional electronic spectroscopy in condensed phase. *Chin. J. Chem. Phys.* **2018**, *31*, 135–151.
- (106) Weng Yu-Xiang; Wang Zhuan; Chen Hai-Long; Leng Xuan; Zhu Rui-Dan. Quantum coherence measurement with femtosecond time-resolve two-dimensional electronic spectroscopy: Principles, applications and outlook. *Acta Phys. Sin.* **2018**, *67*, 127801.
- (107) Wang, R.; Zhang, C.; Zhang, Z.; Li, Y.; Wang, X.; Xiao, M. In *Ultrafast coherent hole transfer in non-fullerene OPV blends*; Conference on Lasers and Electro-Optics, San Jose, California, 2018/05/13; Optical Society of America: San Jose, CA, 2018; p JTh2A.151.
- (108) Son, M.; Mosquera-Vázquez, S.; Schlau-Cohen, G. S. Ultrabroadband 2D electronic spectroscopy with high-speed, shotto-shot detection. *Opt. Express* **2017**, *25*, 18950–18962.
- (109) Mewes, L.; Ingle, R. A.; Al Haddad, A.; Chergui, M. Broadband visible two-dimensional spectroscopy of molecular dyes. *J. Chem. Phys.* **2021**, *155*, 034201.
- (110) Cai, Y.; Wei, Z.; Song, C.; Tang, C.; Huang, X.; Hu, Q.; Dong, X.; Han, W. Novel acceptor—donor—acceptor structured small molecule-based nanoparticles for highly efficient photothermal therapy. *Chem. Commun.* **2019**, *55*, 8967—8970.